ISSN 1023-1935, Russian Journal of Electrochemistry, 2023, Vol. 59, No. 10, pp. 707–713. © Pleiades Publishing, Ltd., 2023.
Russian Text © The Author(s), 2023, published in Elektrokhimiya, 2023, Vol. 59, No. 10, pp. 547–553.

Study of Properties of the Cobalt–Manganese Spinel-Based Coatings Obtained by the Non-Stationary Electrolysis[1]

A. V. Khramenkova[a], *, A. A. Yakovenko[a], K. R. Yuzhakova[a], V. I. Mishurov[b], K. G. Abdulvakhidov[c], and O. E. Polozhentsev[c]

[a] *Platov South-Russian State Polytechnic University (NPI), Novocherkassk, Russia*
[b] *Rostov-on-Don State Technical University, Rostov-on-Don, Russia*
[c] *Southern Federal University, Rostov-on-Don, Russia*
**e-mail: anna.vl7@yandex.ru*

Received November 29, 2022; revised February 10, 2023; accepted March 21, 2023

Abstract—Coatings based on cobalt–manganese spinel $(Mn,Co)(Mn,Co)_2O_4$ are obtained on the stainless-steel surface by polarization with asymmetric alternating current. The study of their mechanical properties showed that the coatings have sufficiently high adhesion to the substrate, their thickness is about 30 μm, and their microhardness value of 40 HV is comparable to that of similar oxide materials. The study of thermal stability in air showed them being stable at temperatures up to 1000°C; the study of corrosion-protective properties, in 3.5 wt % NaCl solution.

Keywords: non-stationary electrolysis, cobalt–manganese spinel, protective coatings
DOI: 10.1134/S1023193523100075

INTRODUCTION

Nowadays, solid-oxide fuel cells gain an increasingly strong foothold among the devices for energy conversion thanks to their environmental friendliness and high effectiveness [1, 2]. One of the solid-oxide fuel cell key component is the interconnectors that, in addition to the providing of electrical contact between elements, prevent a fuel-with-oxidant direct mixing [3]. Generally, the interconnectors are manufactured of ferritic stainless steels whose negative exploitation consequence is the high-temperature formation of chrome volatile compounds, which can lead to the cathode material poisoning.

A problem-solving method is deposition of protective coatings onto the interconnector surface. To this purpose, transition-metal- and oxide-based coatings are used [1]. Nickel coatings at the ferrite-steel-surface were shown [4] to be effective in the course of operational-life testing in the standard operating mode of solid-oxide fuel cells thanks to the formation of Cr_2O_3 grains at the boundary between the stainless steel and the coating; the grains prevent further interdiffusion of the steel and the coating material. The possibility of using Sr-doped conversion $LaFeO_3$-coatings with the perovskite structure as protective coatings for the interconnectors was studied in work [5]. Alkaline-earth-metal cations were shown to exert positive effect on the specific surface resistivity upon the 300-h-testing.

Of special interest are cobalt- and manganese-oxide-based coatings with spinel structure thanks to their high thermal and electrical conductivity and the capability of conversing the chrome components into less volatile compounds, to lower the corrosion rate, as well as the equality of their thermal-expansion coefficient to that of the steel [6, 7].

The analysis of the protective properties of the coatings based on the Co–Mn-spinel with different stoichiometry [8–14] allows claiming their high effectiveness in the sequestering of the chrome volatile compounds as compared with the strontium- and lanthanum-containing coatings with the perovskite structure. Also, it is known that the best operational properties are demonstrated by the mixed spinel-based coatings that have tetragonal and cubic structure at same time [14].

Nowadays, such coatings used to be prepared by physical vapor deposition [15], dipping [16], and electrophoretic deposition [17]. The above-mentioned methods of the coatings' preparation are well energy consuming because their realization requires additional thermal treatment of thus formed coatings up to the formation of Co–Mn complex oxides with the spinel structure.

In this context, there stands out the method of non-steady-state electrolysis based on the using of

[1] Delivered at the 20th All-Russian Meeting "Electrochemistry of Organic Compounds" (EKhOS-2022), Novocherkassk, October 18–22, 2022.

alternating (symmetrical, asymmetrical, or pulse) current. During the using of the non-steady-state electrolysis modes, the oxide coatings are formed in one stage because of the repeatability of the polarizing voltage: during the cathodic half-period, metals are deposited; during the anodic one, oxidized. It is known that the key-role in the metal and metal oxide deposition processes in the non-steady-state mode is played by the usage of different forms of alternating current [18]. In particular, we distinguish between sinusoidal alternating current with cut-off, asymmetrical quasi-sinusoidal alternating current, biased sinusoidal alternating current, and a square-wave pulsed current with galvanostatic or potentiostatic pulses. Additionally, in the preparation of high-purity coatings of great interest is the asymmetrical alternating current that allows controlling the deposited layer composition and properties by purely electrical stimulus [19]. We have gathered experience in the using of the asymmetrical sinusoidal alternating current for the preparation of various-application functional coatings [20].

According to literature data [21], to obtain coatings based on the cobalt and manganese complex oxides, we took the following electrolyte basic components: cobalt nitrate, manganese sulfate, and nickel salts and boric acid. It is known that nickel ions can serve as homogeneous catalysts for cobalt deposition [22]; the boric acid, a buffer additive.

In this work, we aimed at a carrying out of a one-stage synthesis of the Co–Mn-spinel based coatings at the stainless-steel-surface by using the non-steady-state electrolysis and studying of their morphology, phase composition, and thermal stability. The scientific novelty of the study is a new approach to the coating synthesis by using asymmetrical alternating current.

EXPERIMENTAL

The coatings were formed at a pre-treated sample surface with the using of asymmetrical alternating current of commercial frequency (50 Hz) comprising two semisinusoidal waves with different amplitude. The current source was a device comprising two diodes connected in parallel and passing the current in opposite directions via adjustable resistances. The electrochemical cell was a thermostatted glass electrolyzer, 200 mL in volume; the deposition was carried out at the electrolyte constant agitation with a magnetic stirrer.

The working electrodes were macroelectrodes of stainless steel (brand name AISI 430) sized 30 × 20 × 0.2 mm (both sides), the counter-electrode was nickel (brand name NPA1, GOST 492-2006). The ratio of the amplitudes averaged over the cathodic and anodic current period was $I_C : I_A = 1 : 1.25$. The electrolysis temperature was 40°C; the electrolysis time, 60 min. The electrolyte composition was, g L^{-1}: cobalt nitrate ($Co(NO_3)_2 \cdot 6H_2O$)—190.00; nickel nitrate ($Ni(NO_3)_2 \cdot 6H_2O$)—20.00; nickel chloride ($NiCl_2 \cdot 6H_2O$)—20.00; boric acid (H_3BO_3)—30.00; manganese sulfate ($MnSO_4 \cdot 5H_2O$)—25.00.

All solutions were prepared by of reagent grade chemicals and distilled water in the following manner: firstly, the cobalt nitrate was dissolved; then, all the rest of the components, namely the nickel nitrate, nickel chloride, boric acid, and manganese sulfate. The electrolyte solution was agitated with a magnetic stirrer; the solution pH was 3.5–4.0. All experiments were carried out in the 35–40°C temperature interval.

The coating morphology and phase composition was studied without any pre-treatment by using a Quanta 200 scanning electron microscope with tungsten cathode (from the Nanotekhnologii core facilities center of the South-Russian State Polytechnic University (NPI)) with the energy-dispersive X-ray analysis (EDX) option; an INCA Energy software was used.

The coatings' X-ray diffraction analysis was carried out with the using of an ARL X'tra (2007) powder X-ray diffractometer equipped with an energy-dispersive detector and temperature chambers TTK-450 (the temperature interval from –180 to 450°C) and NTK-1000 (from 25 to 1000°C). The X-radiation source was a Cu–X-ray tube with maximal power of 2000 W. The imaging was carried out with a CuK_{α_1}-radiation (the wavelength 1.5406 Å) at a rate of 5 deg/min. X-ray diffractograms were deciphered by using a Pwc 2.3 full-profile program pack.

The coatings' structure and phase composition were also studied by the electron diffraction method using a Zeiss Libra 200FE transmitting electron microscope (the chamber length 567 mm at the accelerating voltage of 200 kV, the resolution 0.12 nm) (from the Nanotekhnologii core facilities center of the St. Petersburg State University). To this purpose, the coating was specially prepared as disperse powder that was applied to the surface of a technical titanium foil (brand name VT1-0) in optimal regime. The coating can be easily removed from the foil as disperse powder because of the extremely low adhesion to the substrate.

The coating thermal stability was studied by the complex thermal analysis method. The analysis was carried out using a NETZSCH STA 449F5 instrument in Pt–Rh-crucibles annealed at a temperature of 1000°C. The crucibles were mounted at the holder sensor surface. The thermal stability of the obtained coatings was studied over the 50–900°C temperature range in oxidative medium (air). The heating rate was 10 K min^{-1}.

The coatings' microhardness was determined by an ITV-1-MM hardness measuring instrument (OOO Metrotest); the thickness, by a Konstanta K5 thickness indicator with an ID1 conversion unit (OOO KONSTANTA).

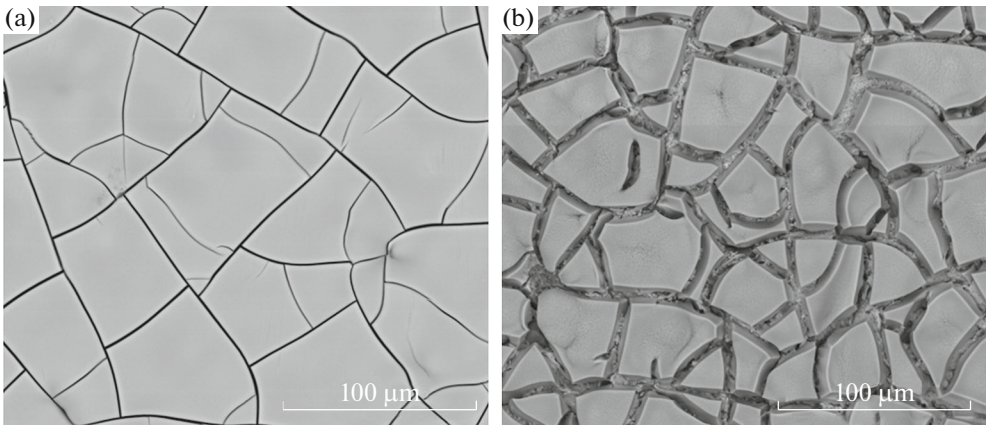

Fig. 1. SEM-images of coating prior to thermal treatment (a) and after treatment (b).

The coating adhesion was evaluated by cross-cut test in accord with the GOST 9.302–88.

The resistances were measured by a ST2558 four-probe tester. To measure the coatings' resistivity, aquadag electrodes were coated on both sides of their surfaces and the full resistance was measured. The resistivity was found by the following formula:

$$\rho = \frac{RS}{d},$$

where R is the difference of the full resistance and that of the metal substrate, S is the electrode surface area, d is the coating thickness.

Polarization measurements were carried out with a P-40X potentiostat/galvanostat (Elins, Russia) equipped with a standard three-electrode electrochemical cell. The studied sample surface area was 1 cm^2. The reference electrode was a silver/silver chloride electrode; the counter-electrode, platinum. Polarization curves were taken over the potential range from −500 to 200 mV at a potential scanning rate of 1 $mV\,s^{-1}$ in the 3.5 wt % NaCl solution. The corrosion potential and corrosion current were determined analytically from the cross-section of the obtained Tafel curves.

RESULTS AND DISCUSSION

It is known that interconnectors of solid-oxide fuel cells' operate over the 600–800°C temperature range [23]. Therefore, the studying of surface morphology and structural features of the protective coatings for the solid-oxide fuel cells' interconnectors is necessary for the prognosis of their behavior in oxidative atmosphere. For this reason, we compared the surface morphology and element composition of the obtained coatings subjected to thermal treatment and those untreated (Fig. 1). The thermal treatment temperature of 800°C was chosen as the upper temperature limit in the interconnector operation.

We see from Fig. 1a that the morphology of the coatings not exposed to the thermal treatment has a mosaic structure that is characteristic of the transition metal oxides; it can be caused by the misfit of the thermal expansion coefficients of the coating material and the substrate metal [24].

Upon the coatings' thermal treatment at 800°C in air, their surface morphology changed drastically (Fig. 1b). We observed the cracks' formation and broadening, accompanied with the decrease in the geometrical size of the mosaic structure fragments.

The analysis of the coatings' element composition (Table 1) showed that the thermal treatment resulted in a decrease of the oxygen concentration; the manganese concentration increased; here, unlike the thermally non-treated coatings, the surface layer contained traces of chrome and iron.

The transition metal oxides contacting air are known to be able generating molecular oxygen upon their heating [25]. This fact can explain the decrease of the oxygen concentration upon the thermal treatment. The increase in the manganese concentration can be explained by the change in its valence and formation of a new chemical state [26]. In addition, after the ther-

Table 1. Data of the energy-dispersive X-ray analysis of the coatings

Element	Chemical composition of coating surface, at %	
	prior to thermal treatment	after thermal treatment
O	67.3	49.1
Mn	28.5	38.5
Co	3.8	4.0
Ni	0.3	–
Cr	–	2.7
Fe	–	5.7

mal treatment we observed the presence of chrome and iron. The former can be the consequence of the chrome diffusion from the steel and its fixation by the coating's components; the presence of iron can be connected with the change in the coating morphology and the cracks' broadening, which allowed identifying the iron from the substrate.

Prior to the carrying out of the X-ray diffraction analysis, the obtained coatings were subjected to the thermal treatment at 200°C up to the reaching constant mass, in order to remove different forms of the bound water. However, we failed in the determining of the phase composition because of the X-ray-amorphous character of the obtained coatings (Fig. 2, curve *1*). In X-ray patterns of the coating subjected to the thermal treatment at 500° C (Fig. 2, curve *2*), we also observed only spread-out peaks which did not allow their deciphering. Only, the thermal treatment at 800°C produced the well-defined well-crystallized structure (Fig. 2, curve *3*).

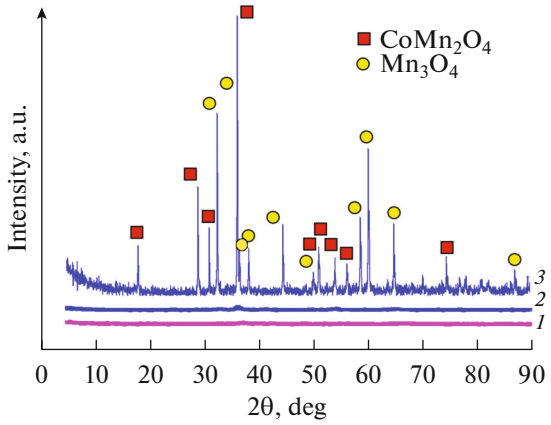

Fig. 2. X-ray diffraction patterns of coatings thermally pretreated at temperatures of, °C: (*1*) 200, (*2*) 500, (*3*) 800.

Table 2. X-ray diffraction data of the coatings

Compound	2θ exp.	2θ theor.	*d*, Å exp.	*d*, Å theor.
1	2	3	4	5
$CoMn_2O_4$	18.09	18.16	4.90	4.88
	29.04	29.35	3.07	3.04
	31.11	30.89	2.87	2.89
	36.22	36.07	2.48	2.49
	36.66	36.81	2.45	2.44
	51.12	51.07	1.79	1.79
	52.58	52.73	1.74	1.74
	54.09	54.00	1.69	1.70
Mn_3O_4	32.56	32.38	2.75	2.76
	36.22	36.08	2.48	2.49
	38.32	38.09	2.35	2.36
	44.56	44.41	2.03	2.04
	50.15	50.84	1.82	1.80
	58.72	58.50	1.57	1.58
	60.2	59.91	1.54	1.54
	64.6	64.61	1.44	1.44

In this case, the basic phases of the coating are Mn_3O_4 and $CoMn_2O_4$ (cards no. 80-0382 and no. 77-0471 from the PDF2 database, respectively) (Table 2).

To determine the phase composition of the thermally non-treated coatings, we additionally used the electron diffraction method. In Fig. 3a we give a transmitting-electron-microscopy-image of an area of the coating at which the electron diffraction was measured (Fig. 3b).

In the electronogram (Fig. 3b), all reflections are rather broad, which also states that the particles are nano-sized (10–15 nm). Identified interplanar spaces (1.5 and 2.5 nm) correspond to the mixed-type spinel

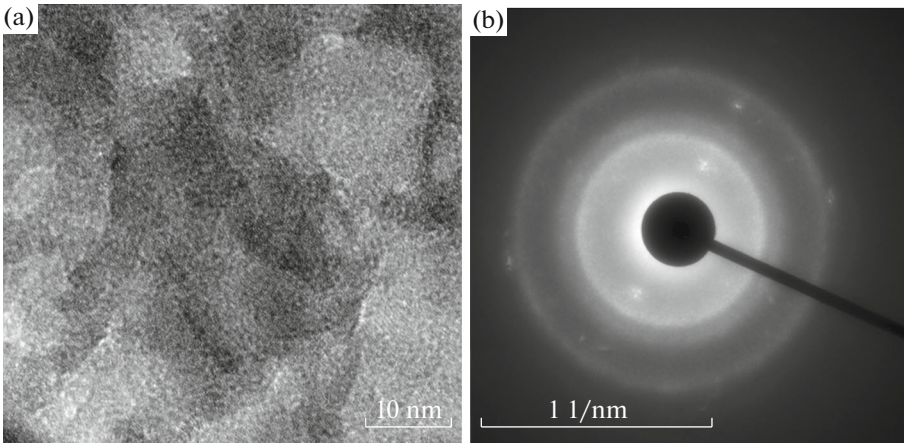

Fig. 3. TEM-image (a) and X-ray diffraction pattern (b) of coating.

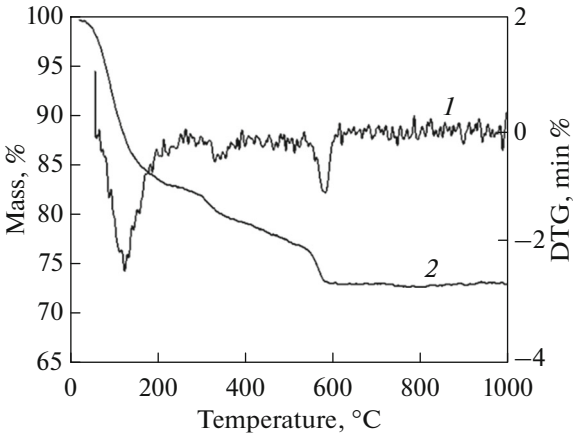

Fig. 4. Results of the study of the coatings' thermal stability in oxidative environments.

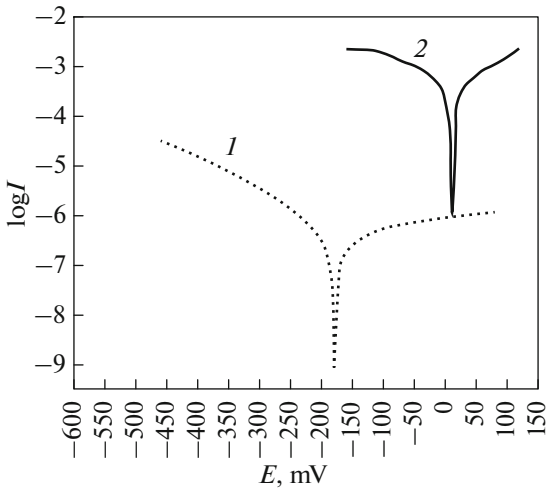

Fig. 5. Potentiodynamic polarization curves taken in 3.5% NaCl for uncoated steel (*1*) and coating (*2*).

$(Mn,Co)(Mn,Co)_2O_4$ that can be thought of as a mixture of $MnCo_2O_4$ and $CoMn_2O_4$ [27].

The comparison of the data obtained by the electron diffraction and X-ray diffraction analysis showed them to be closely correlated.

The coatings' thermal behavior was studied in air over the 50–1000°C temperature interval (Fig. 4, curve *1*). In the differential thermal analysis curve, we observed two well-pronounced endothermic peaks at 95 and 570°C. The first peak corresponds to the loss of the crystallization water. It is known that at 570°C the complex oxide $(Mn,Co)(Mn,Co)_2O_4$ can be converted to $CoMn_2O_4$ and manganese oxide Mn_3O_4, which is accompanied by oxygen evolution [28]. The observed endothermic peak is likely to correspond to this phenomenon.

The water loss in the thermogram (Fig. 4, curve *2*) corresponds to three temperature intervals. The first one is located below 250°C; it is accompanied by the mass loss up to 18% and is connected with the crystallization water loss. The second temperature interval is accompanied by the mass loss up to 28%, which may be caused by the removal of different forms of the bound water and the cobalt–manganese complex oxide phase transition. Upon reaching 570°C, no mass loss has been observed.

The study of the corrosion-protective properties of the obtained coatings demonstrated their effectiveness in 3.5% NaCl solution (Fig. 5). The obtained polarization curves showed well-pronounced rectangular fragments in Tafel coordinates, which allowed determining the corrosion potential and corrosion current. Upon the coating deposition, we observed a shift of the corrosion potential toward more positive values. In particular, the E_{cor} values for the uncoated steel and the coating were −179.1 and 12.5 mV; the I_{cor} values, 3.98×10^{-7} and 3.16×10^{-4} mA, respectively. The difference of the I_{cor} values for the coating and uncoated steel can be explained by the change in the structure of deposited coating, more precisely, by the cracks' broadening and the partial revealing of the metal substrate. This lowered the coating blocking functions; the electrolyte can concentrated near the cracks, which leads to the steel local corrosion that used to proceed more intensely as compared with the uniform corrosion.

The study of adhesion by cross-cut test showed that upon the providing a net of scratches the coatings have not been delaminated from the substrate, which corresponds to zero point after GOST 31149–2014. The synthesized coating are 30–35 μm-thick. Their microhardness is 40 HV; the resistivity, 7832 Ω m.

CONCLUSIONS

(1) The using of the asymmetrical alternating current allowed forming cobalt–manganese-spinel-based coatings on the stainless-steel surface in one stage. Their morphology is mosaic.

(2) The obtained coatings are shown to be thermally and corrosion-stable. Their microhardness is as high as 40 HV.

FUNDING

This work was financially supported by the UMNIK-Tekhnokrat program of the Innovation Promotion Fund, the contract no. 17527GU/2022.

CONFLICT OF INTEREST

The authors declare that they have no conflict of interest.

REFERENCES

1. Agarkova, E.A., Agarkov, D.A., Burmistrov, I.N., et al., Three-Layered Membranes for Planar Solid Oxide Fuel Cells of the Electrolyte-Supported Design: Characteristics and Applications, *Russ. J. Electrochem.*, 2020, vol. 56, p. 132.
2. Tan, K.H., Rahman, H.A., and Taib, H., Coating layer and influence of transition metal for ferritic stainless steel interconnector solid oxide fuel cell: A review, *Int. J. Hydrogen Energy*, 2019, vol. 44, no. 58, p. 30591.
3. Zanchi, E., Talic, B., Sabato, A.G., Molin, S., Boccaccini, A.R., and Smeacetto, F., Electrophoretic co-deposition of Fe_2O_3 and $Mn_{1,5}Co_{1,5}O_4$: Processing and oxidation performance of Fe-doped Mn–Co coatings for solid oxide cell interconnects, *J. Eur. Ceram. Soc.*, 2019, vol. 39, p. 3768.
4. Demeneva, N.V. and Bredikhin, S.I., Oxide film formation and diffusion processes in near-surface layers of current collectors in solid oxide fuel cells, *Russ. J. Electrochem.*, 2014, vol. 50, p. 725.
5. Frangini, S., Della Seta, L., and Paoletti, C., Preparation and Electrical Properties of Sr-Doped $LaFeO_3$ Thin-Film Conversion Coatings for Solid Oxide Cell Steel Interconnect Applications, *Energies*, 2022, vol. 15, p. 632.
6. Yu, Y.T., Lu, Y., Guan, C.Z., Wang, J.Q., and Zhu, J.H., Evaluation of the reactive-sintered $(Mn,Co)_3O_4$ spinel layer for SOFC cathode-side contact application, *Int. J. Hydrogen Energy*, 2022, vol. 47, no. 87, p. 36964.
7. Yiqian, J., Guozheng, H., Mengyuan, G., Wangshu, H., Jiaqi, Sh., Zhibin, Y., Xingyu, X., and Suping, P., Ce-doped $(Mn,Co)_3O_4$ coatings for solid oxide fuel cell interconnect applications, *Ceram. Int.*, 2022, vol. 48, no. 23, p. 34931.
8. Wei-Ja, Sh., Chien-Kuo, L., Wei-Xin, K., Yung-Neng, Ch., and Ruey-Yi, L., High temperature (800°C) oxidation of AISI 441 stainless steel with Mn–Co contact layers for SOFC stacks, *Int. J. Hydrogen Energy*, 2022, vol. 47, p. 6811.
9. Puranen, J., Pihlatie, M., Lagerbom, J., Bolelli, G., Laakso, J., Hyvärinen, L., Kylmälahti, M., Himanen, O., Kiviaho, J., Lusvarghi, L., and Vuoristo, P., Post-mortem evaluation of oxidized atmospheric plasma sprayed Mn–Co–Fe oxide spinel coatings on SOFC interconnectors, *Int. J. Hydrogen Energy*, 2014, vol. 39, p. 17284.
10. Dogdibegovic, E., Ibanez, S., Wallace, A., Kopechek, D., Arkenberg, G., Swartz, S., Funk, J. M., Reisert, M., Rahman, M. A., Aphale, A., Singh, P., Ding, H., Tang, W., Glazoff, M. V., Ding, D., Skafte, Th. L., and Tucker, M. C., Performance of stainless steel interconnects with $(Mn,Co)_3O_4$-Based coating for solid oxide electrolysis, *Int. J. Hydrogen Energy*, 2022, vol. 47, p. 24279.
11. Tomas, M., Asokan, V., Puranen, J., Svensson, J.-E., and Froitzheim, J., Efficiencies of cobalt- and copper-based coatings applied by different deposition processes for applications in intermediate-temperature solid oxide fuel cells, *Int. J. Hydrogen Energy*, 2022, vol. 47, p. 32628.
12. Reddy, M.J., Chausson, T.E., Svensson, J.E., and Froitzheim, J., 11–23% Cr steels for solid oxide fuel cell interconnect applications at 800°C – How the coating determines oxidation kinetics, *Int. J. Hydrogen Energy*, 2023.
13. Zhikuan, Zh., Chibuzor, D.-U., Uday, P., Srikanth, G., Mohammed, H. A., Nilesh, D., Yosuke, F., Yohei, M., Yutaro, M., and Soumendra, B., Comparison of Cu–Mn and Mn–Co spinel coatings for solid oxide fuel cell interconnects, *Int. J. Hydrogen Energy*, 2022, vol. 47, p. 36953.
14. Brylewski, T., Kucza, W., Adamczyk, A., Kruk, A., Stygar, M., Bobruk, M., and Dąbrowa, J., Microstructure and electrical properties of $Mn_{1+x}Co_{2-x}O_4$ ($0 \le x \le 1.5$) spinels synthesized using EDTA-gel processes, *Ceram. Int.*, 2014, vol. 40, p. 13873.
15. Jia, C., Wang, Y., Molin, S., Zhang, Y., Chen, M., and Han, M., High temperature oxidation behavior of SUS430 SOFC interconnects with Mn-Co spinel coating in air, *J. Alloys Compd.*, 2019, vol. 787, p. 1327.
16. Li, J., Xiong, C., Li, J., Yan, D., Pu, J., Chi, B., and Jian, L., Investigation of $MnCu_{0.5}Co_{1.5}O_4$ spinel coated SUS430 interconnect alloy for preventing chromium vaporization in intermediate temperature solid oxide fuel cell, *Int. J. Hydrogen Energy*, 2017, vol. 42, p. 16752.
17. Aznam, I., Mah, J.C.W., Muchtar, A., Somalu, M.R., and Ghazali, M.J., Electrophoretic deposition of $(Cu,Mn,Co)_3O_4$ spinel coating on SUS430 ferritic stainless steel: Process and performance evaluation for solid oxide fuel cell interconnect applications, *J. Eur. Ceram. Soc.*, 2020, vol. 41, p. 1360.
18. Kireev, S.Yu., Yangurazova, A.Z., Kireeva, C.N. Effect of different non-steady-state electrolysis modes on the rate of electroplated coating formation by metals and alloys, their composition and properties (in Russian), *Izv. Vuzov, Volga District*, 2017, vol. 4, p. 86.
19. Shul'gin, L.P., *Electrochemical Processes in Alternating Current* (in Russian), Leningrad: Nauka, 1974.
20. Khramenkova, A.V., Ariskina, D.N., and Yuzhakova, K.R., Production of Hybrid Polymer-Oxide Materials Based on Molybdenum Oxide Compounds Using Transient Electrolysis Method, *Solid State Phenom.*, 2020, vol. 299, p. 316.
21. Mingyu, L., Jin, X., Wei, G., Zhaolin, Zh., and Zulai, L., Effect of yttrium on the oxidation resistance and area specific resistance of $MnCo_2O_4$ coating, *Surf. Coat. Technol.*, 2022, vol. 444, p. 128655.
22. Bespalova, J.I., Khramenkova, A.V., Abdala, R.M., and Dmitriev, V.P., Study of the phase composition and structure of composite coatings based on transition-metal oxide compounds via X-ray diffraction and X-ray absorption fine structure spectroscopy, *J. Surf. Investig. X-ray, Synchrotron Neutron Techniques*, 2014, vol. 8, p. 60.
23. Yan, Y., Bateni, R., Harris, J., and Kesler, O., Fabrication of reactive element oxide coatings on porous ferritic stainless steel for use in metal-supported solid oxide fuel cells, *Surf. Coat. Technol.*, 2015, vol. 272, p. 415.

24. Zhu, W.Z. and Deevi, S.C., Development of interconnect materials for solid oxide fuel cells, *Mater. Sci. Eng.*, 2003, vol. 348, p. 227.

25. Boikov, E.V., Vishnetskaya, V., Emel'yanov, A.N., Rufov, Yu.N., and Shcherbakov, N.V.,Partial oxidation of benzene at transition metal oxides deposited onto silica gel, *Khim. Fizika*, 2007, vol. 26, p. 38 (in Russian).

26. Anan'ev, V., Solodyankin, A.A., Eremin, V.A., Farlenkov, A.S., Khodimchuk, A.V., Fetisov, A.V., Chernik, A.A., Yaskel'chik, V.V., Ostanina, T.N., and Zaikov, Yu.P., Protective coatings of La–Mn–Cu–O on a 08X17T steel-interconnector for solid-oxide fuel cells obtained by electrocrystallization from nonaqueous electrolyte solutions (in Russian), *Izv. Vuzov, Tsvetnaya Metallurgiya*, 2017, vol. 6, p. 70.

27. Zhu, J. H., Chesson, D. A., and Yu, Y. T., Review—$(Mn,Co)_3O_4$-Based Spinels for SOFC Interconnect Coating Application, *J. Electrochem. Soc.*, 2021, vol. 168, p. 114519.

28. Feng, Q., Yanagisawa, K., and Yamasaki, N., Hydrothermal Soft Chemical Process for Synthesis of Manganese Oxides with Tunnel Structures, *J. Porous Mater.*, 1998, vol. 5, p. 153.

Translated by Yu. Pleskov